CONCEPT FOR SOFT-LINKING A MULTI-ENERGY SYSTEM CO-PLANNING MODEL TO AN URBAN ENERGY SIMULATION PLATFORM

C. B. Heendeniya[1], S. Köhler[1], B. Schröter[1]
[1]University of Applied Sciences - Stuttgart, Stuttgart, Germany

ABSTRACT

Soft-linking multi-energy system (MES) models with urban energy simulation platforms (UESP) enable high spatial resolution modeling of local energy systems. The smallest energy unit of an urban MES model is the "building energy-hub" that describes the interaction between different energy carriers in a building. A building also represents a data structure that consists of geometrical, topological, and semantic information in a UESP.

In this paper, we present a concept and first results of a simple urban use-case for soft-linking MES models and UESP. The potential to extend this method to model the interactions among many prosumers is also discussed.

SYMBOLS

Sets:

T = Set of time-steps

I = Set of technologies

Parameters:

η_{bat} = Battery efficiency

$P_{bat}^{ch,max}, P_{bat}^{dc,max}$ = Max. battery charge and discharge rates

Ω_{ramp} = Max. heat pump ramp rate

$\boldsymbol{\varphi_{grid}^{CO2}, \varphi_{dhn}^{CO2}}$ = Emission factors for electricity and district heating

$\boldsymbol{\lambda_{inv}, \lambda_{op}, \lambda_{feed}}$ = Investment, operation, and feed-in costs

$\boldsymbol{\lambda_{grid}, \lambda_{dhn}}$ = Energy purchase cost from grid and district heating network

Variables:

P_{grid} = Power import from the grid

$\boldsymbol{P_{hp}}$, $\boldsymbol{P_{el}}$ = Heat pump and building elect. demand

$P_{bat}^{ch}, P_{bat}^{dc}$ = Charge/ discharge power of battery

Q_{dhn} = Heat import from district heating network

Q_{hp}, S_{hp} = Heat pump energy for space heating and hot water generation

Q_{heat}, S_{hw} = Heating and hot water energy demand

Q_{tess}^{ch}, Q_{tess}^{dc} = Charge/ discharge power of thermal storage

S_{hw}^{ch}, S_{hw}^{dc} = Charge/ discharge power of hot water buffer storage

H_{pv} = PV generation

$P_{pv}, P_{feed}, P_{curt}$ = PV consumption, feed-in, and curtailment

COP_{hp} = Heat pump efficiency

SoC_{bat} = Battery state-of-charge

C_{bat}, C_{hp} = Battery and heat pump installed capacity

INTRODUCTION

Energy system co-planning models combine the characteristics of expansion and operation planning models, whereby the expansion decisions are determined by considering the operational aspects of the energy system. The requirement for considering operational details of the energy system in the expansion planning process stems from the increase of variable renewable energy generation and the smart-grid technologies in the energy system. The weather-dependent energy production, behavior dependent demand, and incentive-driven control strategies directly influence the future technology mix we require to achieve the economic optimality while meeting other technical and environmental requirements.

A recent review article by (Heendeniya et al., 2020) discusses the status-quo of district-scale energy system co-planning models. The article identifies key challenges and the future research potential for modeling district-scale multi-energy systems (MES), in which multiple energy vectors dynamically interact

 DOI: 10.3217/978-3-85125-786-1-74

with each other that discussed under three main aspects.

1. Temporal resolution.
2. Energy system and network models.
3. Spatial granularity.

(Heendeniya et al., 2020) further emphasizes that linking MES co-planning models with UESP, enable more comprehensive and high-resolution evaluation of energy scenarios in the districts. Some examples of the state-of-the-art UESP and their capabilities to represent energy network and multi-energy couplings are shown in Table 1.

Table 1: Energy network and multi-energy interaction modeling capabilities of some existing UESP.

REF.	ENERGY NETWORK MODEL	MULTI-ENERGY COUPLINGS
Hong et al, 2016	None	No
Reinhart et al, 2013	None	No
Bergerson et al, 2015	None	No
Nageler et al, 2017	District heating only	No

This contribution builds on top of the insights from (Heendeniya et al., 2020), attempts to conceptualize a method to couple MES co-simulation with the UESP SimStadt. SimStadt uses 3D CityGML files as the primary input and connects the geometric, semantic, and topological data from CityGML files to several databases and libraries. The calculation of building energy demands and renewable energy potentials is performed by the INSEL simulation engine (Nouvel et al., 2015). Figure 1 shows a graphical overview of SimStadt and (Weiler et al., 2019) provides a comprehensive description of the architecture and the current applications of SimStadt.

In the proposed concept, each building in the neighborhood is represented by an equivalent energy-hub model and a mixed-integer optimization algorithm is implemented to evaluate the optimal co-planning strategy for each of the building. The buildings may interact with each other and with the external energy system through the energy network.

The objective of this contribution is to,

1. present the broad concept for soft-linking SimStadt and MES co-simulation model,
2. discuss the necessity to model part-load performance of distributed generators, and present a methodology to accomplish that,
3. present a simple use-case of a single-building energy-hub that soft-links with SimStadt UESP,
4. share future directions and potential for multi-disciplinary research collaborations.

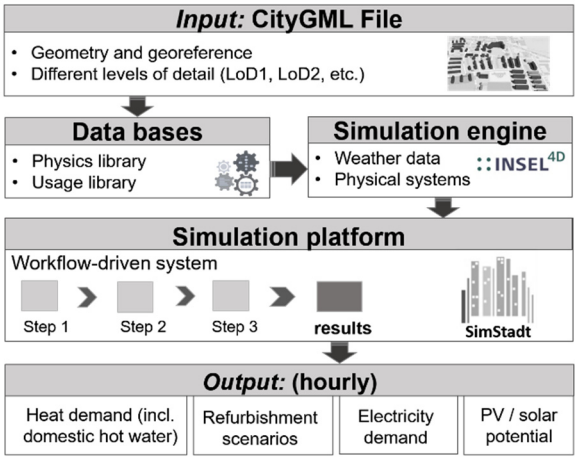

Figure 1: Simplified structure of SimStadt with inputs and outputs

CONCEPT AND METHODOLOGY

Overview

Figure 2 shows one (simple) way of conceptualizing the district-scale MES co-simulation within an UESP. The architecture in figure 1 has several sub-modules that generates/ forecasts energy demand profiles for each building. The generated demand and renewable generation profiles are stored in a cloud-based data platform accessible to the MES co-simulation model.

Figure 3 illustrates the energy-hub model of a single building. The energy-hub models represent electricity, heating, and domestic hot water energy demand vectors. The energy supply vectors are the utility network for electricity, heat, and renewable energy from solar photovoltaics. It also models the charging and discharging of the battery and thermal storage and power-to-heat conversion via a ground-source heat pump (GSHP).

Mathematical model

This section explains the mathematical representation of the energy-hub model and the co-planning optimization problem for a single building.

The mathematical representation of the energy-hub model captures the fundamental demand and supply balances for each energy carrier and the conversion between energy carriers.

Equation 1-3 describe the energy balance equations for electricity, heat, and hot water at each time-step in the planning period. The most common application of building-scale battery storage is to improve the self-consumption of renewable generation. Thermal storage is used to store heat from power-to-heat conversion. These intentions are described using the binary decision variables $x_{bat}^{ch}(t), x_{bat}^{dc}(t), x_{tess}^{ch}(t), x_{tess}^{dc}(t), x_{hw}^{ch}(t), x_{hw}^{dc}(t)$ that indicate whether a charging or discharging action occurs for each type of storage at each time-step. We implement a quadratic formulation of the energy

 DOI: 10.3217/978-3-85125-786-1-74

balance equations with the above-mentioned decision variables to constrain the battery and thermal storages from being charged by grid electricity supply and district heating supply.

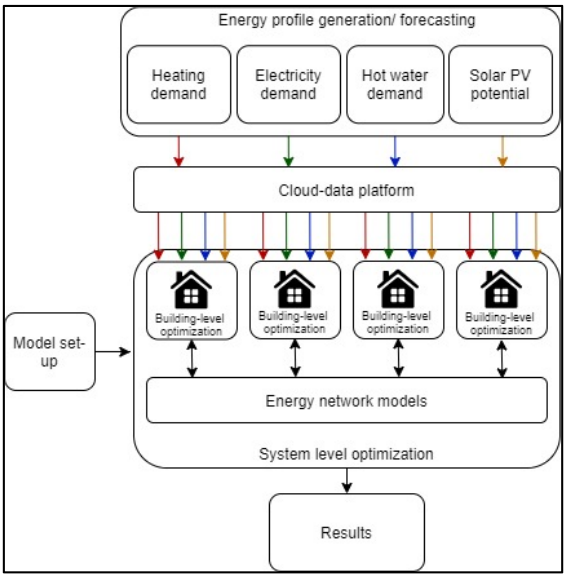

Figure 2: Concept for neighborhood-scale energy simulations by coupling a MES co-optimization model and an UESP.

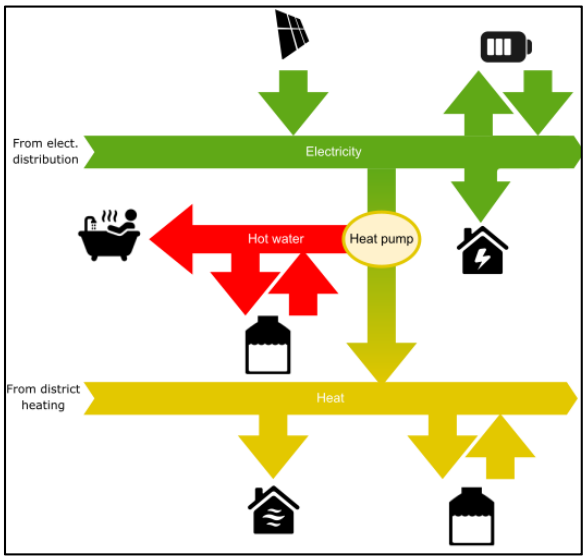

Figure 3: The energy-hub representation of the multi-energy system for a single building.

$$\begin{aligned} &P_{grid}(t).\left(1-x_{bat}^{ch}(t)\right)+P_{pv}(t)\\ &-P_{bat}^{ch}(t).x_{bat}^{ch}(t)\\ &+P_{bat}^{dc}(t).x_{bat}^{dc}(t)\\ &-P_{hp}(t)-P_{el}(t) \end{aligned} = 0 \quad (1)$$

$$\begin{aligned} &Q_{dhn}(t).\left(1-x_{tess}^{ch}(t)\right)\\ &-Q_{tess}^{ch}(t).x_{tess}^{ch}(t)\\ &+Q_{tess}^{dc}(t).x_{tess}^{dc}(t)\\ &+Q_{hp}(t)-Q_{heat}(t) \end{aligned} = 0 \quad (2)$$

$$\begin{aligned} &-S_{hw}^{ch}(t).x_{hw}^{ch}(t)+S_{hw}^{dc}(t).x_{hw}^{dc}(t)\\ &+S_{hp}(t)-S_{hw}(t) \end{aligned} = 0 \quad (3)$$

$$\forall\, t \in T$$

The renewable electricity from PV must be either consumed (directly or via storage), fed back to the grid, or curtailed (equation 4). The PV power feed-in at any time-step t should be less than the maximum power feed-in.

$$H_{pv}(t)-P_{feed}(t)-P_{curt}(t)=P_{pv}(t) \quad (4)$$

$$\forall\, t \in T$$

The conversion of one energy carrier to another is characterized by the corresponding conversion efficiency. Equation 5 describes the relationship between the thermal output of the GSHP and its electrical input. The COP depends on the loading of the heat pump at each time-step, as shown by equation 6. Here, $\gamma_{hp}(t)$ is the part-load level of the GSHP at time t and $C_{hp}(t)$ is the installed capacity of the GSHP.

$$Q_{hp}(t)+S_{hp}(t)=COP_{hp}(t).P_{hp}(t) \quad (5)$$

$$Q_{hp}(t)+S_{hp}(t)=\gamma_{hp}(t).C_{hp} \quad (6)$$

$$\forall\, t \in T$$

The relationship between the part-load level and the COP is shown in figure 4, which is mathematically modelled using a piece-wise linear approximation.

The dynamics of charging and discharging the energy storage is described in equations 7-8.

$$\begin{aligned} &SoC_{bat}(t-1)+P_{bat}^{ch}(t).x_{bat}^{ch}(t).\eta_{bat}\\ &-P_{bat}^{dc}(t).x_{bat}^{dc}(t).\eta_{bat} \end{aligned} = \mathrm{SoC}_{bat}(t) \quad (7)$$

$$\forall\, t \in T \text{ and } t \neq 1$$

$$\begin{aligned} &P_{bat}^{ch}(t).x_{bat}^{ch}(t).\eta_{bat}\\ &-P_{bat}^{dc}(t).x_{bat}^{dc}(t).\eta_{bat} \end{aligned} = \mathrm{SoC}_{bat}(t) \quad (8)$$

$$\forall\, t \in T \text{ and } t = 1$$

 DOI: 10.3217/978-3-85125-786-1-74

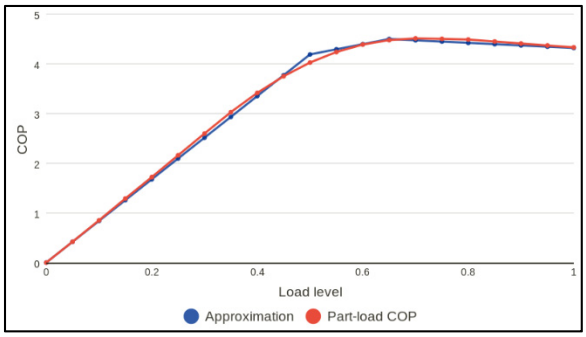

Figure 4: Part-load efficiency variation of the GSHP.

The time-step resolution is not explicitly shown in equations 7-8, because in this case-study, we use one-hour time-steps. The state-of-charge of battery storage at time t is limited to the installed capacity of the battery storage (equation 9) and the charging and discharging power is limited to the maximum charge/ discharge power (equations 10-11). The storage dynamics for thermal and hot water buffer storages are modeled similarly.

$$\mathrm{SoC}_{bat}(t) \leq C_{bat} \tag{9}$$

$$P_{bat}^{ch}(t) \leq P_{bat}^{ch,max} \tag{10}$$

$$P_{bat}^{dc}(t) \leq P_{bat}^{dc,max} \tag{11}$$

$$\forall\, t \in T$$

The ability of the heat pump to increase and decrease its electrical power input (hence the thermal power output) is a useful source of flexibility for the local power distribution network (Fischer et al, 2017).

$$\Omega_{ramp} \leq Q_{hp}(t) + S_{hp}(t) - Q_{hp}(t-1) - S_{hp}(t-1) \tag{12}$$

$$-\Omega_{ramp} \geq Q_{hp}(t) + S_{hp}(t) - Q_{hp}(t-1) - S_{hp}(t-1) \tag{13}$$

$$\forall\, t \in T \text{ and } t \neq 1$$

The equations 12 and 13 define the maximum heat pump power-up and power-down (ramp) rate constraints.

The total amount of CO_2 emissions that results from the MES operation is calculated by equation 14. Here, φ_{grid}^{CO2} and φ_{dhn}^{CO2} are the CO_2 emission factors of the electricity distribution and district heating, respectively (equation 12).

$$\sum_{t\in T} \mathrm{P}_{grid}(t).\left(1 - x_{bat}^{ch}(t)\right).\varphi_{grid}^{CO2} + \sum_{t\in T} Q_{dhn}(t).\left(1 - x_{tess}^{ch}(t)\right).\varphi_{dhn}^{CO2} = \pi_{CO2} \tag{14}$$

The total cost of the MES co-planning is the annualized sum of the investment, operation, and energy purchase costs. In equations 15-19, σ_{inv}, σ_{op}, σ_{en}, and σ_{fit} are the total investment cost, operation cost, energy cost, and feed-in revenue for the planning horizon. The technology life time and the discount rate are given by n and r, respectively.

$$\sum_{\iota\in \mathrm{I}} C(\iota).\lambda_{inv}(\iota)\left[\frac{r.(1+r)^{n(\iota)}}{(1+r)^{n(\iota)}-1}\right] = \sigma_{inv} \tag{15}$$

$$\sum_{t\in T}\sum_{\iota\in \mathrm{I}} P(\iota,t).\lambda_{op}(\iota) = \sigma_{op} \tag{16}$$

$$\sum_{t\in T} \mathrm{P}_{grid}(t).\left(1 - x_{bat}^{ch}(t)\right).\lambda_{grid} + \sum_{t\in T} \mathrm{P}_{dhn}(t).\left(1 - x_{tess}^{ch}(t)\right).\lambda_{dhn} = \sigma_{en} \tag{17}$$

$$\sum_{t\in T} P_{feed}(t).\lambda_{feed} = \sigma_{fit} \tag{18}$$

$$\sigma_{inv} + \sigma_{op} + \sigma_{en} - \sigma_{fit} = \sigma_{total} \tag{19}$$

The optimization objective of the co-planning problem is to minimize the total cost σ_{total}.

$$Obj.function = Min.\ \sigma_{total} \tag{20}$$

PART-LOAD EFFICIENCY MODELING

Significance of part-load efficiency curve modeling

The part-load operation and short cycling conditions result in the efficiency degradation of heat pumps (Waddicor et al., 2016). The heating and hot water demand in buildings can be significantly time-varying; therefore, it can impose highly variable loading conditions on the heat pump. The effect of variable loading conditions on the heat pump depends on the sizing and the operating strategy of the heat pump. In other words, by choosing the optimal size and the operation strategy for the heat pump, it is possible to minimize the loss of efficiency at part-load conditions. Therefore, MES co-planning models must consider the variation of heat pump efficiency under variable loading conditions.

Piece-wise linear approximation of the GSHP part-load efficiency curve

This subsection provides a detailed explanation of the piece-wise linear approximation of the GSHP part-load efficiency curve.

Piece-wise linear approximation of a non-linear function can be evaluated by sampling the non-linear function into several "pieces" and then calculating the linear curve-fitting of the non-linear function inside the domains represented by those pieces. In our co-planning model, the part-load efficiency curve of the GSHP is a piece-wise linear approximation function with three pieces.

To model the piece-wise linear approximation, we introduce a set of four weight variables W and a set of four binary decision variables Y (equations 21-22). Assuming (α_1, β_1), (α_2, β_2), (α_3, β_3), and (α_4, β_4) are

 DOI: 10.3217/978-3-85125-786-1-74

the breakpoints of the three linear segments, we can model the piece-wise linear approximation as shown in the equations 23-30.

$$W = \{w_i | w_i \in \mathbb{R}^+, 0 \leq w_i \leq 1, i = 1,2,3,4\} \quad (21)$$

$$Y = \{y_i | y_i \in \{0,1\}, i = 1,2,3,4\} \quad (22)$$

$$COP_{hp}(t) = \sum_i \beta_i . w_i(t) \quad (23)$$

$$\gamma_{hp}(t) = \sum_i \alpha_i . w_i(t) \quad (24)$$

$$1 = \sum_{t \in T} w_i(t) \quad (25)$$

$$2 \geq \sum_{t \in T} y_i(t) \quad (26)$$

$$y_i(t) \geq w_i(t) \quad (27)$$

$$1 \leq y_1(t) + y_3(t) \quad (28)$$

$$1 \leq y_1(t) + y_4(t) \quad (29)$$

$$1 \leq y_2(t) + y_4(t) \quad (30)$$

$$\forall\, t \in T$$

CASE-STUDY

The case study is a multi-family building in Stuttgart - Germany (figure 5). The building has;

- a footprint area of 2,311m²,
- a total roof area of 2,366m² and,
- a heated area of 6,174m².

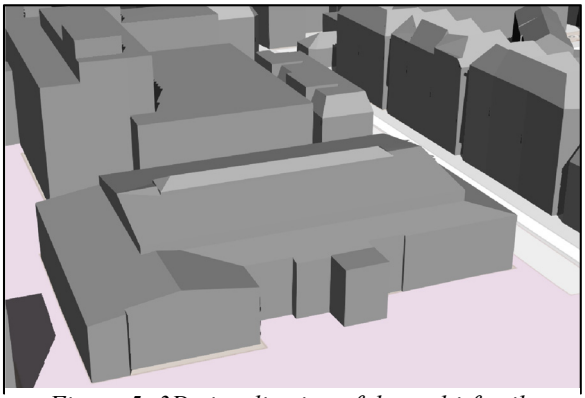

Figure 5: 3D visualization of the multi-family building in Stöckach.

Each of the four stories of the building has an average height of 3.3 meters. The building contains 77 households and a total occupancy of 152 people. The total yearly heat demand (incl. domestic hot water) is estimated at 320.12MWh/a, and the electricity demand is 215.46MWh/a. The heating demand is calculated with DIN 18599, using parameters, like U-values from the German Building Typology (Loga et al., 2015). This building is specified with a year of construction in 2002 and has an average U-value of 0.39 W/(m²K). Other key model parameters are given in Table 2.

Table 2: Key model parameters.

MODEL PARAMETER	VALUE
Rated HP COP	4.47
Thermal storage efficiency	0.90
Hot water buffer storage efficiency	0.90
Battery storage efficiency	0.95
Electricity cost	0.30 EUR/kWh
District heating cost	0.10 EUR/kWh
Investment costs:	
- PV roof top	1000 EUR/kW
- Heat pump	1400 EUR/kW
- Battery storage	1066 EUR/kW
- Thermal (and buffer) storage	60 EUR/kW
Operation cost:	
- PV roof top	0
- Heat pump	0.001 EUR/kWh
- Battery storage	0.005 EUR/kWh
- Thermal (and buffer) storage	0.002 EUR/kWh

Figure 6 shows the SimStadt-generated hourly thermal load profile for the whole building. The heating period is set from October to April, while the interior set point temperature is defined with 20°C and the heating limit temperature is set to 15°C. Also, a night-time temperature setback is considered from midnight until 6 am. The highest peak demand is seen on January 12th with 135kW.

Figure 7 and figure 8 show the hourly electricity load profile for a typical winter period (January 1st till January 14th) as well as a typical summer period (June 1st till June 14th). The baseload throughout the year is 10kW, the average at 24.6kW with a minimum/maximum value of 7.3/64.1kW.

Nine roof surfaces with a total area of more than 40m² are considered for the PV potential calculation. Due to practical reasons, smaller surfaces are not taken into consideration. The total available roof area for PV installation, hence, is 2,297m². To model the relationship between the hourly PV production and the installed capacity, we normalize the hourly PV generation potential with an area requirement of 6m²/kWp. A set of 2880 representative time-steps (one month per season) is selected to keep the computational time within a reasonable limit.

The optimization problem is modeled in python programming language and solved using Gurobi 9.0.0 (academic license) solver.

 DOI: 10.3217/978-3-85125-786-1-74

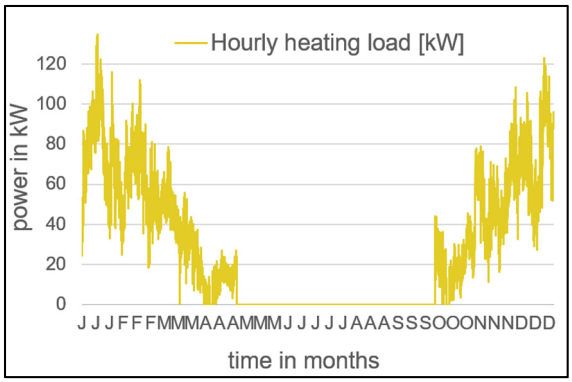

Figure 6: Hourly heating demand of the building for an entire year.

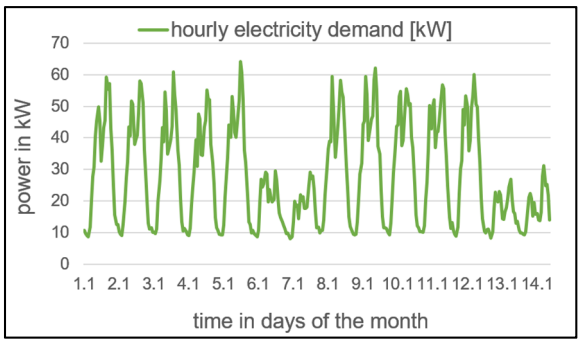

Figure 7: Hourly electricity demand of the building for two winter weeks.

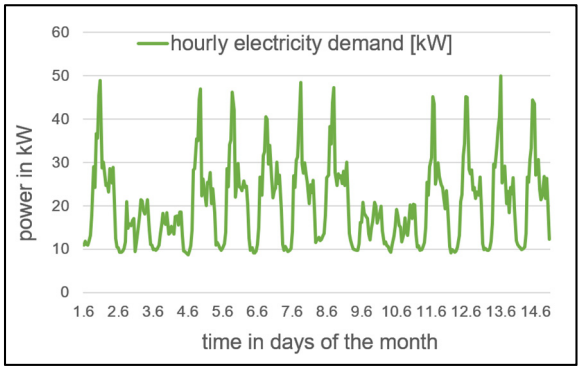

Figure 8: Hourly electricity demand of the building for two summer weeks.

RESULTS

We compared the results of the MES model with and without implementing the part-load efficiency variation of the heat pump. In the latter, the heat pump efficiency is equal to its maximum rated efficiency at every time-step.

Influence of part-load modelling on thermal storage

Table 3 shows the optimal value calculated by the MES co-planning model for four different decision variables when the heat pump part-load efficiency variation is considered and when not. The most significant difference that we observe is in the optimal sizing of thermal and buffer storages. This observation is intuitive because when there is no penalty for the low part-load operation of the heat pump, the benefits of thermal and buffer storage to improve heat pump capacity utilization are not well-demonstrated. The resulting unfavorable cost-benefit balance hinders the installation of thermal and buffer storage.

Table 3:

The optimal value calculated for various model variables with and w/o heat pump part-load efficiency variation.

MODEL VARIABLE	WITH PART-LOAD EFF. VARIATION	W/O PART-LOAD EFF. VARIATION
HP capacity	47.3 kW_{th}	45.9 kW_{th}
Thermal storage capacity	10.0 kWh	0.0 kWh
Hot water buffer storage capacity	262.3 kWh	247.8 kWh
Heat import from district heating network	32.5 MWh	34.2 MWh

Influence of part-load modelling on heat pump operation

The variation of the heat pump loading for the first 1200 time-steps of the simulation for time-varying and constant efficiency is shown in figure 9 and figure 10.

From the part-load efficiency curve in figure 4, we observe that the heat pump efficiency curve is relatively flat between 60 – 100% loading. Below the 60% load level, the efficiency drops rapidly.

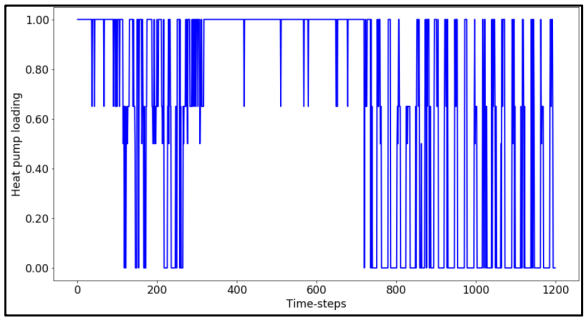

Figure 9: Heat pump loading over the first 1200 time-steps of the simulation under time-varying efficiency.

Figure 9 shows the influence of having an efficiency penalty for low part-load operation. In contrast to not having an efficiency penalty for low part-load operation (figure 10), we see that the heat pump tends to adjust its operating point to maintain approx. 60 - 100% loading the majority of the time. The thermal storage system provides the required flexibility so that the heat pump can optimally adjust its operating point (figure 11). On the flip-side, this may result in a higher

 DOI: 10.3217/978-3-85125-786-1-74

number of on-off sequences of the heat pump, as the heat pump tends to shut down entirely at low loading conditions.

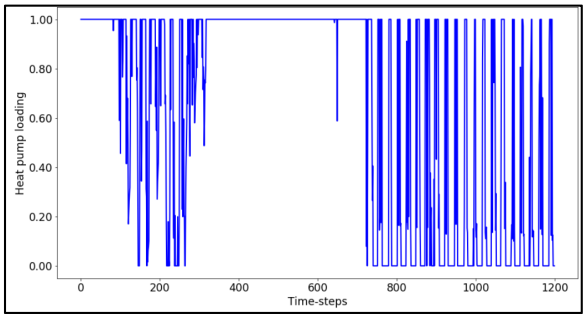

Figure 10: Heat pump loading during the first 1200 time-steps under constant efficiency.

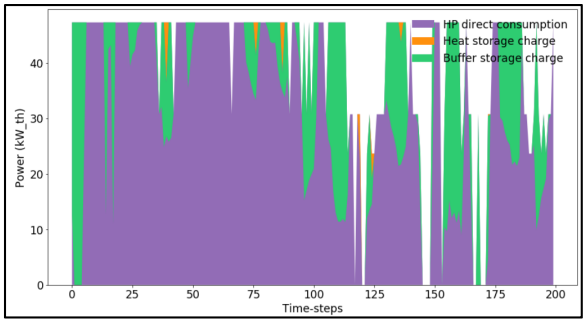

Figure 11: The direct consumption and charging of heat and hot water buffer storage with heat pump thermal energy output for the first 200 time-steps of the simulation with part-load efficiency modelled.

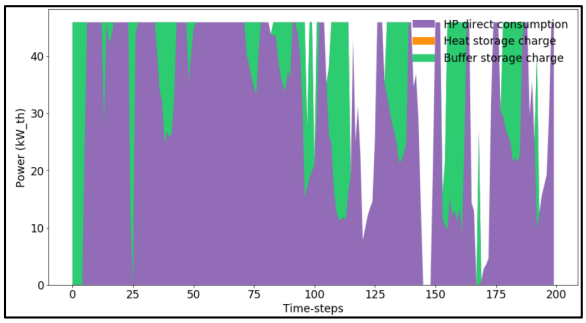

Figure 12: The direct consumption and charging of heat and hot water buffer storage with heat pump thermal energy output for the first 200 time-steps of the simulation at constant heat pump efficiency.

The ill-significances of the rapid heat pump on-off cycles are, 1) the degradation of the heat pump and 2) the negative effect on the local electricity distribution due to high starting current.

Influence of the ramp constraint on heat pump operation

Table 4 shows the optimal value for a set of selected decision variables with and without a maximum heat pump ramp limit of 2% (of the installed capacity) per time-step. The results show that the sizing of the technologies is not affected by the ramp constraint.

Table 4:
The optimal value calculated for various model variables with and w/o heat pump part-load efficiency variation.

MODEL VARIABLE	WITH RAMP CONSTRAINT	W/O RAMP CONSTRAINT
HP capacity	45.9 kW_{th}	45.9 kW_{th}
Thermal storage capacity	0.0 kWh	0.0 kWh
Hot water buffer storage capacity	247.8 kWh	247.8 kWh
Heat import from district heating network	34.4 MWh	34.2 MWh

The ramping constraint reduces the number of rapid on-off cycles that we observed previously.

Figure 13 shows that the ramping constraint, without the part-load efficiency variations, could lead to the heat pump operating more frequently at very low part-load conditions.

The stack plot in figure 14 shows the shares of the thermal energy output of the heat pump that is directly consumed and used to charge thermal and hot water buffer storage for the first 200 time-steps (for clear visualization).

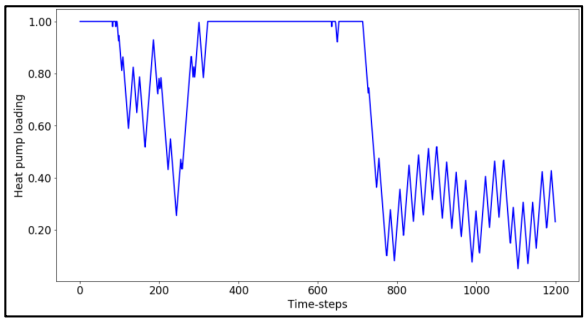

Figure 13: Variation of heat pump loading during the first 1200 time-steps with constant heat pump efficiency and 2% maximum ramp rate.

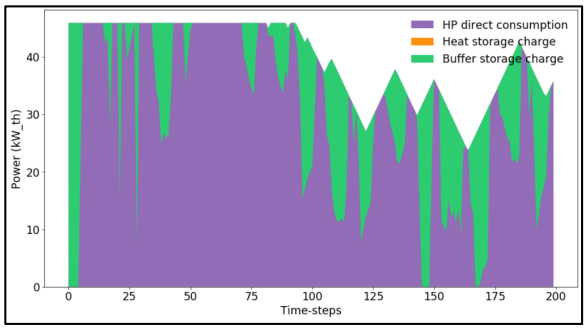

Figure 14: The direct consumption and charging of heat and hot water buffer storage with heat pump thermal energy output for the first 200 time-steps of the simulation with 2% maximum ramp rate.

 DOI: 10.3217/978-3-85125-786-1-74

DISCUSSION AND CONCLUSION

The two main arguments to why part-load efficiency variation of heat pumps must be considered in MES co-planning models are; firstly, it influences the cost-optimal scheduling of the heat pump and secondly it enables demonstration of the load-shifting benefits of thermal storage systems in the energy system to improve heat pump capacity utilization.

The heat pump ramping constraint, on the other hand, sets a threshold to heat pumps ability to follow the thermal demand. Whether the ramping constraint significantly affect the operating flexibility of the heat pump depends on the thermal demand profile of the building.

Frequent on-off cycles of the heat-pump reduces the life-time of the heat pump and unfavorable for the power system. Such effects can only be visualized by integrating a dynamic power system model in the future.

The main challenge of soft-linking UESP and MES optimal co-planning models are the scalability. The run-time of mixed integer optimization models grows exponentially as the increasing number of decision variables, which is the case when the number of simulated buildings increase. One of the ways to lower the computational burden is to carefully select the minimum number of representative time-steps by considering the trade-offs between the required solution accuracy for the given co-planning objective and the computational burden. This method, although widely popular, does not reduce the complexity of the problem structure.

A hierarchical structure to the optimization problem that aligns better with the microgrid control architecture is also interesting to look at. In such an architecture, the optimization problem maybe defined at the system, building, and the heat pump level taking into account the key planning decisions that needs to be taken at each hierarchical level. The planning horizon, inputs, and constrains can be defined only as relevant to each hierarchical level; therefore, reducing the complexity.

ACKNOWLEDGEMENT

The lead author is supported by M4_LAB. M4_LAB is a transfer project at the University of Applied Sciences - Stuttgart within the framework of the "Innovative Hochschule" initiative funded by the Federal Ministry of Education and Research under the grant number 03IHS032A. We also wish to thank Ruben Pesch for the insightful discussions and support.

REFERENCES

Heendeniya, C. B., Sumper, A., & Eicker, U. (2020). The multi-energy system co-planning of nearly zero-energy districts – Status-quo and future research potential. In *Applied Energy*, 267. https://doi.org/10.1016/j.apenergy.2020.114953

Hong, Tianzhen; Chen, Yixing; Lee, Sang Hoon; Piette, M. (2016): CityBES: A Web-based Platform to Support City-Scale Building Energy Efficiency. In *Urban Computing* (14), p. 2016.

Reinhart, C.; Dogan, Timur; Jakubiec, J.; Rakha, Tarek; Sang, Andrew (2013): UMI - An urban simulation environment for building energy use, daylighting and walkability. In *Proceedings of BS 2013: 13th Conference of the International Building Performance Simulation Association*.

Bergerson, Joshua; Muehleisen, Ralph; Rodda, Bo; Auld, Joshua; Guzowski, Leah; Ozik, J.; Collier, Nicholson (2015): Designing Future Cities – LakeSIM Integrated Design Tool For Assessing Short- and Long-Term Impacts of Urban Scale Conceptual Designs. In *ISOCARP Review* 11, pp. 48–63.

Nageler, P.; Zahrer, G.; Heimrath, R.; Mach, T.; Mauthner, F.; Leusbrock, I. et al. (2017): Novel validated method for GIS based automated dynamic urban building energy simulations. In *Energy* 139, pp. 142–154. DOI: 10.1016/j.energy.2017.07.151.

Nouvel, R., Brassel, K. H., Bruse, M., Duminil, E., Coors, V., Eicker, U., & Robinson, D. (2015). SimStadt, a new workflow-driven urban energy simulation platform for CityGML city models. *CISBAT 2015 Proceedings, 889-894*

Weiler, V., Stave, J., & Eicker, U. (2019). Renewable Energy Generation Scenarios Using 3D Urban Modeling Tools—Methodology for Heat Pump and Co-Generation Systems with Case Study Application. *Energies*, 12(3), 403. doi: 10.3390/en12030403

Fischer, D., & Madani, H. (2017). On heat pumps in smart grids: A review. *Renewable and Sustainable Energy Reviews*, *70*, 342–357. doi: 10.1016/j.rser.2016.11.182

Orehounig, K., Evins, R., & Dorer, V. (2015). Integration of decentralized energy systems in neighbourhoods using the energy hub approach. *Applied Energy*, *154*, 277–289. doi: 10.1016/j.apenergy.2015.04.114

Waddicor, D. A., Fuentes, E., Azar, M., & Salom, J. (2016). Partial load efficiency degradation of a water-to-water heat pump under fixed set-point control. *Applied Thermal Engineering*, *106*, 275–285. doi: 10.1016/j.applthermaleng.2016.05.193

Loga, T., Stein, B., Diefenbach, N., & Born, R. (2015). Deutsche Wohngebäudetypologie Beispielhafte Maßnahmen zur Verbesserung der Energieeffizienz von typischen Wohngebäuden. *Darmstadt: Wohnen und Umwelt*.

 DOI: 10.3217/978-3-85125-786-1-74